ARTICLE NO. 79-0282R

J80-069

Three-Dimensional Flow over Wings with Leading-Edge Vortex Separation

00001
20005
20016

F. T. Johnson* and E. N. Tinoco†
Boeing Aerospace Company, Seattle, Wash.
and
P. Lu‡ and M. A. Epton‡
Boeing Computer Services, Inc., Seattle, Wash.

Recent advances in a panel method for the solution of three-dimensional flow about wing and wing-body combinations with leading-edge vortex separation are presented. These advances were achieved as part of an ultimately successful assault on two shortcomings of the method, namely convergence failures in seemingly random cases, and overprediction of lift coefficient for high aspect-ratio wings. Advances include the implementation of improved panel numerics for the purpose of eliminating the highly nonlinear effects of ring vortices around doublet panel edges, and the development of a least-squares procedure for damping vortex sheet geometry update instabilities. A variety of cases generated by the computer program implementing the method are presented. These cases are of two types. The first type consists of numerical studies, which verify the underlying mathematical assumptions of the method and moreover show that the results are strongly invariant with respect to such user dependent input as wing panel layout, initial sheet shape, sheet rollup, etc. The second type consists of cases run for the purpose of comparing computed results with experimental data, and these comparisons verify the underlying physical assumptions made by the method.

Nomenclature

a = tangent basis vector
A = compressibility matrix
$\mathcal{R}$ = aspect ratio
b = local span
B = boundary of fluid domain
c = chord
C_D = drag coefficient
C_ℓ = rolling moment coefficient
C_L = lift coefficient
C_M = pitching moment coefficient
C_N = normal force coefficient
C_P = pressure coefficient
D = fluid domain
F = equations determining singularity parameters
F = force vector
G = equations determining geometry parameters
H = hyperboloidal panel
K = equations penalizing panel twist
ℓ = panel width
$\hat{\ell}$ = unit vector along vortex core or network junction
L = curve on B across which μ is discontinuous
M_∞ = freestream Mach number
$\hat{n}$ = surface unit normal vector
n = normal vector at panel center
n_c = surface co-normal vector
p = pressure
p_i = isentropic pressure
p_2 = second-order pressure
P = field point
Q = point on boundary B
Q_i = nine canonical panel points
Q_0 = panel center
Q_s, Q_t, Q_{st} = parametric coefficients defining H
R = compressible magnitude of R
R = vector from Q to P
s,t = hyperboloidal surface parameters
S = singularity surface
v = perturbation velocity
V = total velocity
V_A = average surface value of total velocity
V_∞ = freestream velocity magnitude
V_∞ = freestream velocity
w = perturbation mass flux vector
W = total mass flux vector
W_A = average surface value of total mass flux vector
$\hat{x}$ = unit vector along x axis
x,y,z = Cartesian coordinates
α = angle of attack
β = $\sqrt{1-M^2}$
γ = delta wing semi-apex angle
Δ = jump in quantity across singularity surface or line or change in quantity from one iteration to the next
ζ = surface vorticity vector
η = span fraction
θ = vortex system orientation angles
Θ = all vortex systems geometry parameters
λ = vortex system scale factor
Λ = all singularity parameters
μ = doublet strength
μ_i = doublet strength at Q_i
ν = fed sheet scale factor
ξ = chord fraction aft of trailing edge

Presented as Paper 79-0282 at the AIAA 17th Aerospace Meeting, New Orleans, La., Jan. 15-17, 1979; submitted Feb. 20, 1979; revision received Aug. 31, 1979.

Index categories: Aerodynamics; Computational Methods; Subsonic Flow.

*Research Scientist, BMAD Aerodynamics Staff. Member AIAA.
†Specialist Engineer, BMAD Aerodynamics Staff. Member AIAA.
‡Specialist Mathematician, Energy Technology Application Division.

ρ = fluid density
ρ = Newton iteration step size limits
ρ_∞ = freestream fluid density
σ = source strength
ϕ = perturbation potential
(ϕ_x,ϕ_y,ϕ_z) = gradient of perturbation potential
∇ = gradient operator
$\tilde{\nabla}$ = cogradient operator
ϵ = belongs to

I. Introduction

THE flow at the leading and tip edges of a swept wing with sharp edges separates at moderate to high angles of attack, the separation producing vortex sheets that roll up into strong vortices above the upper surface of the wing. The formation of these vortices is responsible for the well-known nonlinear aerodynamic characteristics exhibited over the angle-of-attack range. Experimental studies[1] of the vortex sheet separating from a slender sharp-edged wing revealed that the rolled-up part of the vortex sheet consists of three regions: an outer, convection dominated region in which the distance between turns is large compared to the diffusion distance; an inner region where the distance between turns is of the same order of magnitude as the diffusion distance; and an inner, diffusion-dominated, viscous core which is very small, representing only about 5% of the vortex diameter. In addition, studies[1,2] of the principal vortex indicate that its shape and strength are relatively independent of Reynolds number. The relative lack of viscosity dependence suggests that the flow may be regarded as potential, with the free shear layer represented either as a vortex sheet or, equivalently, a doublet distribution, supporting a discontinuity in tangential velocity.

Background

Many theoretical methods have exploited this fact to predict various flow characteristics. The leading-edge-suction analogy described in Refs. 3-5 provides a method suitable for calculating the magnitude of the nonlinear vortex lift on a rather broad class of wing planforms. Polhamus[3] reasoned that the normal force needed for the flow around a leading edge to reattach to the wing is equivalent to the leading edge suction force necessary to force the flow to be attached to the edge in an unseparated condition. The unseparated leading edge suction force is calculated, and is then rotated normal to the wing to obtain the lift contribution of the leading edge vortex. The total wing lift computed by this method agrees well with experimental data, but the leading-edge-suction analogy does not give flowfield details or detailed surface pressure distributions. Several attempts had been made in the past toward the theoretical prediction of detailed pressure distributions and flowfields about swept wings with leading edge vortex separation. Most of these past methods are limited to slender configurations, a considerable simplification because the problem can be reduced to a solution of Laplace's equation in the cross flow plane, for which conformal mapping becomes a powerful tool. Smith[6] developed the best known method of this type by improving the work done earlier in collaboration with Mangler.[7] Assuming conical flow, which is approximately valid near the apex of the wing, he was able to predict qualitatively the type of pressure distributions that had been observed experimentally. Those pressure distributions exhibit a vortex-induced pressure peak at about 70% of the local semispan of the wing. Toward the trailing edge, Smith's method overpredicts the experimental load distribution by a considerable amount, because the conical theory does not satisfy the Kutta condition at the trailing edge. Conical flow methods were followed by fully three-dimensional techniques in which the vortex is represented by single or multiple line vortices[8-13] or by a vortex sheet,[14-16] and in which the trailing edge Kutta condition is enforced. These methods have enjoyed reasonable success in predicting overall configuration forces and moments and in some cases wing pressure distributions. A current review of various methods is presented in Ref. 17.

The method considered in this paper is basically that of Ref. 15. This method is capable of predicting forces, moments and detailed surface pressures on wing and wing-body combinations assuming the separation lines are known. The wing geometry may be arbitrary in the sense that leading and trailing edges may be curved or kinked and the wing may have arbitrary camber and twist as long as in real flow it produces only a single well developed vortex system. The method employs an inviscid flow model in which the configuration surface is represented by source and/or doublet singularity panels, and the rolled-up vortex sheets and wakes are represented by doublet panels alone. The Kutta condition is imposed along all wing edges. Strengths of the singularities as well as shape and position of the free vortex sheet spirals are computed iteratively starting with an assumed initial sheet geometry. The method has been in use for some time now with generally good results, however certain shortcomings have become apparent. First, the iterations determining sheet shape and position have become unstable in seemingly random cases, making parametric studies difficult.[18] Minor changes in wing paneling, for example, have sometimes caused a well converged case to diverge. Second, computed lift coefficients for wings of large aspect ratio have tended to be higher than those predicted by the suction analogy and experiment.[18] The effort to solve these problems is summarized in the following section.

Approach to the Problem

The convergence problem was addressed first in the hope of creating a more reliable tool for investigating the aspect ratio problem. To improve confidence in the numerical features of the method a general upgrade of the numerics was made. The upgrade included such minor things as a more precise calculation of the geometry and network edge matching sensitivities, but the major effort was the implementation of parametrized panels and doublet splines in order to ensure continuity of geometry and doublet singularity strength across all panel edges, thereby eliminating the highly non-linear effects of line vortices (discontinuities in doublet strength). This upgrade did indeed enlarge the class of problems over which convergence was achieved; nevertheless, some rather simple cases still diverged. It was, therefore, necessary to look at more fundamental possibilities. A detailed analysis of divergence indicated that because of certain paneling anomalies, satisfaction of some of the boundary conditions required rather substantial kinks in the vortex sheet locally which, as pointed out by Rubbert, set off a built-in instability in the vortex sheet updating procedure. A very simple least-squares penalty technique was developed to damp this instability with the result that convergence was achieved in all of a wide variety of previously diverged cases to which the technique was applied.

It has been the authors' belief that the lift coefficient calculated by the current method should tend to agree with those of the suction analogy wherever the assumptions of that theory are valid, hence, the attack on the second problem began with studies designed to check the numerical implementation of the method. These studies included the determination of the effect of variations in panel density, panel layout, sheet roll-up, initial sheet shape, etc. In all cases the studies proved that the boundary value problem associated with the model was being solved quite accurately so that the model itself was in error. It was discovered subsequently that use of the linearized pressure formula in the wing wake (known to be somewhat inadequate at low aspect ratios) was causing substantial loss of the wing trailing edge Kutta condition at high aspect ratios. The use of a fixed design wake then eliminated the problem and produced ex-

cellent lift coefficient comparisons.

In Sec. II we describe the general features current method as a point of departure for Sec. III, where the advances leading to the solution of the aforementioned problems are detailed. In Sec. IV we give examples of numerical verification of the method and in Sec. V we given examples veryifying the physical assumptions of the model.

II. Description of the Method

Theoretical Model

The essential elements of the present flow model, as outlined in Fig. 1, are the configuration surfaces (wing, body, etc.), the trailing sheet (wake), the sheet emerging from the wing leading edge and tip (free sheet), and the rolled-up core or spiral region (fed sheet) fed by the leading-edge and tip-vortex sheets. The following boundary conditions are imposed on these elements:

1) The configuration surface must be impermeable.

2) The free sheet and wake cannot support a pressure difference and must be impermeable as well.

3) The fed sheet is an extension of the free sheet and feeds vorticity to the vortex core (modeled as a simple line vortex). The boundary condition governing fed sheet size and core orientation is that the total force induced on the fed sheet and core by the rest of the configuration be parallel to the core. The size of the fed sheet is chosen initially by experience or from the conical flow results of Smith.[6]

4) Kutta conditions are imposed along the appropriate leading, side, and trailing edges of the wing in the presence of free sheets emanating from these edges.

Basic Concepts

The Prandtl-Glauert equation

$$\beta^2\phi_{xx}+\phi_{yy}+\phi_{zz}=0 \quad \beta^2=1-M_\infty^2 \tag{1}$$

is assumed to govern the perturbation velocity potential ϕ in the flowfield about the configuration. Here the x axis is taken as the freestream direction, i.e., $V=V_\infty\,\hat{x}$, where V_∞ is the freestream velocity and V its magnitude. Total velocity V is then defined by $V=V_\infty+v$, where $v=(\phi_x,\phi_y,\phi_z)$ is the perturbation velocity. The definition of impermeability and pressure appropriate to Eq. (1) is an open subject. We prefer the mathematically natural choice of zero normal mass flux and the second order pressure formula.[19] The total mass flux vector W is defined as

$$W=\rho_\infty V_\infty+w \tag{2}$$

where w is the perturbation mass flux vector defined by

$$w=\rho_\infty(\beta^2\phi_x,\phi_y,\phi_z) \tag{3}$$

To first order in perturbation quantities $W=\rho V$ (Ref. 19); hence, impermeability can be expressed by

$$(W\cdot\hat{n})=0 \tag{4}$$

where $\hat{n}$ is the surface normal. Equation (1), rewritten as $\nabla\cdot W=0$, expresses conservation of mass, and Eq. (4) then guarantees that even if the configuration is such that the assumptions used to derive Eq. (1) are violated locally there is still no net production of fluid at the boundary surfaces.

The second order pressure formula is

$$p_2=p_\infty-[\rho_\infty(V_\infty\cdot v)+\tfrac{1}{2}(v\cdot w)] \tag{5}$$

and it agrees with the isentropic formula

$$p_i=p_\infty+\frac{\rho_\infty V_\infty^2}{\gamma M_\infty^2}\left\{\left[1-\frac{\gamma-1}{2}\frac{M_\infty^2}{V_\infty^2}(|V|^2-V_\infty^2)\right]^{\frac{\gamma}{\gamma-1}}-1\right\} \tag{6}$$

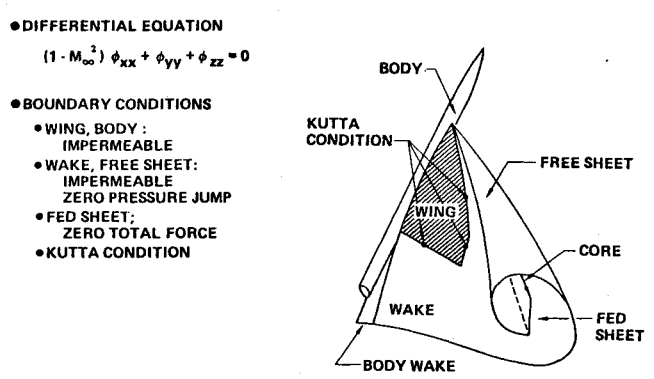

Fig. 1 Flow model.

to first order in perturbation quantities. Mathematically the second order formula is closely associated with Eqs. (1) and (4) in that Eq. (1) is simply the Euler-Lagrange equation for the Bateman variational principle,

$$\iiint_D p_2\,dD=\text{stationary} \tag{7}$$

for which specification of $(W\cdot\hat{n})$ is the natural Neumann boundary condition. Of great importance in our case is that the second order pressure formula produces consistent force calculations for arbitrary configurations when we define force in the usual way, i.e.,

$$F=-\iint_S[V(W\cdot\hat{n})+p_2\hat{n}]\,dS \tag{8}$$

Equation (1) implies that F is zero when the surface S encloses fluid only, hence, momentum is conserved exactly and the force on a given surface may be computed on any enclosing surface.

Under rather general assumptions, Green's third identity[20,21] shows that any solution of Eq. (1) at a field point P may be expressed as the potential induced by a combination of source singularities of strength $\sigma(Q)$ and doublet singularities of strength $\mu(Q)$ on the boundary $Q\epsilon B$ of the fluid domain D:

$$\phi(P)=\iint_B\sigma(Q)\left(\frac{-1}{4\pi R}\right)dS_Q+\iint_B\mu(Q)\hat{n}\cdot\tilde{\nabla}_Q\left(\frac{1}{4\pi R}\right)dS_Q \tag{9}$$

Here R is the position vector $P-Q$, R is the compressible magnitude of R defined by

$$R=\sqrt{R\cdot A\cdot R} \text{ where } A=\begin{bmatrix}1&0&0\\0&\beta^2&0\\0&0&\beta^2\end{bmatrix} \tag{10}$$

and $\tilde{\nabla}_Q$ is the cogradient with respect to Q defined by

$$\tilde{\nabla}_Q=\beta^2A^{-1}\nabla_Q \tag{11}$$

The perturbation velocity $v(P)$ associated with ϕ may be computed by differentiating Eq. (9):

$$v(P)=\iint_B\sigma(Q)\,\nabla_P\left(\frac{-1}{4\pi R}\right)dS_Q+\iint_B\mu(Q)\hat{n}\cdot\tilde{\nabla}_Q\left(\nabla_P\frac{1}{4\pi R}\right)dS_Q \tag{12}$$

whereupon application of Stokes' theorem to the second term on the right yields

$$v(P)=\iint_B \sigma(Q)\,\nabla_P\left(\frac{-1}{4\pi R}\right)dS_Q+\ldots$$

$$\ldots\iint_B \zeta(Q)\times\tilde{\nabla}_Q\left(\frac{1}{4\pi R}\right)dS_Q+$$

$$\ldots\int_L \Delta\mu(Q)\,\tilde{\nabla}_Q\left(\frac{1}{4\pi R}\right)\times d\ell \qquad (13)$$

Here $\zeta(Q)$ is the surface vorticity vector defined by

$$\zeta=\hat{n}\times\nabla\mu \qquad (14)$$

and L is any curve on B across which μ has a discontinuity, say $\Delta\mu$. It is possible to show from Eqs. (8, 9, 12, and 13) that across any singularity surface s

$$\Delta\phi=\mu \qquad (15)$$

$$\hat{n}\times\Delta V=\zeta \qquad (16)$$

$$(\hat{n}\cdot\Delta W)=\rho_\infty\sigma \qquad (17)$$

$$\Delta p_2=-[n_c\cdot(W_A\times\zeta)+(W_A\cdot\hat{n})\sigma]/(\hat{n}\cdot n_c) \qquad (18)$$

and

$$\Delta F=-\iint_S [W_A\times\zeta-V_A\rho_\infty\sigma]dS+\int_L \mu W_A\times d\ell \qquad (19)$$

where Δ denotes the difference between the value on the side on which $\hat{n}$ is defined and the other side, and the subscript A denotes the average of the two values. Here n_c is the co-normal defined by

$$n_c=\beta^2 A^{-1}\hat{n} \qquad (20)$$

Mathematical Implementation of the Model

We now describe the mathematical implementation of the boundary value problem set forth. Our basic unknowns are the source and doublet strengths on all surfaces and the position of the free, fed and wake sheet surfaces. To solve for these unknowns we derive the following equations.

On a surface bounding the fluid on both sides (i.e., thin sheets such as the free sheet, wake and possibly wing) we require that Eq. (4) hold on both sides so that from Eq. (17) we see that such a surface is source free. Hence, we can replace these two boundary conditions by the equivalent conditions that the surface be a doublet surface and that

$$(W_A\cdot\hat{n})=0 \qquad (21)$$

On the wake and free sheet surfaces we have the additional requirement that

$$\Delta p_2\equiv -n_c\cdot(W_A\times\zeta)/(\hat{n}\cdot n_c)=0 \qquad (22)$$

Although both equations involve doublet strength and surface geometry, the primary function of Eq. (22) in conjunction with Eq. (12) is to define surface doublet strength whereas the function of Eq. (21) is to define the surface normal, and, hence, surface geometry. An approximation often made by many methods for wake surfaces is that

$$W_A\approx\rho_\infty V_\infty \qquad (23)$$

in which case Eqs. (22) and (21) determine wake vorticity and surface slope prior to solution. Such an approximation is not precisely valid but, nevertheless, can be made at least in the far wake because details of the wake flow there have little effect on wing pressures. However, a more accurate representation is sometimes required in the near wake, primarily because the spanwise component of vorticity in the near wake (which can be large in that portion of the wake is underneath the primary vortex core) has a strong influence on the Kutta condition at the wing trailing edge. In this case the solution approach used is to require that Eq. (22) be satisfied on fixed wake surfaces in the immediate vicinity of the wing trailing edge, which causes the wake vorticity to seek the correct lateral alignment there.

The Kutta condition at the junction of a (thin) wing and vortex sheet can be stated in several ways; e.g., zero pressure jump at the wing edge, finite flow at the wing edge, no flow through the vortex sheet, etc. All of these phenomena are supposed to occur once the Kutta condition is satisfied, and which boundary condition is actually called the Kutta condition depends on which boundary conditions have previously been assigned to the wing and vortex sheet. In our case we have already assumed that Eq. (21) holds on the wing and Eq. (22) on the sheet, neither of which guarantee finite flow at the wing edge. Infinite flow can be created only by a discontinuity in doublet strength or surface vorticity across the wing/sheet junction. A discontinuity in doublet strength creates a line vortex of strength equal to the discontinuity (Eq. (13). The powerful flow singularity induced by such a vortex is incompatible with wing impermeability and, hence, a discontinuity in doublet strength is already prevented by the wing boundary condition Eq. (21). However, the weak flow singularity induced by a discontinuity in the surface vorticity vector ζ is not. In fact, there exist vorticity distributions creating infinite velocities at the junction, yet no normal mass flux on the wing nor pressure jump on the vortex sheet. These distributions are such that $\zeta\cdot\hat{\ell}$ tends to infinity as the junction is approached from the wing side, where $\hat{\ell}$ is the unit vector along the junction. Thus our choice as the Kutta condition (as originally proposed by Rubbert) is that $\zeta\cdot\hat{\ell}$ be continuous from the wing to the vortex sheet, i.e., that $\Delta\zeta\cdot\hat{\ell}=0$ where $\Delta\zeta=\zeta_{\text{vortex}}-\zeta_{\text{wing}}$. Other components of ζ may be discontinuous, however, these discontinuities will be eliminated by the process of updating the vortex sheet to satify Eq. (21) (which can only happen if the surface normal n is continuous across the junction).

Following Smith,[6] the purpose of the fed sheet is to condense the free sheet vorticity into a line vortex core, thereby terminating the free sheet rollup. Hence, the fed sheet is chosen to be a doublet sheet whose strength is equal to the doublet value at the junction with the free sheet. Only the size and position of the fed sheet remain to be determined from boundary conditions. The boundary conditions are chosen to be consistent with those that would be applicable to the infinitely rolled up vortex sheet as well, namely, that the total force normal to the core be zero, i.e., $\hat{\ell}\times\Delta F=0$ where $\hat{\ell}$ is the unit vector along the line vortex core and ΔF is given by Eq. (19).

On surfaces bounded on one side by a non-fluid domain, e.g., body or thick wing, we require that Eq. (4) hold on the fluid side. While this boundary condition formally completes the mathematical description of the boundary value problem set forth earlier in this section, it is not sufficient to guarantee a unique solution to the problem via Eq. (12) since both source and doublet strength on such surfaces cannot be determined by one boundary condition. However, we can assign a (nearly) arbitrary boundary condition to the other side,[22] in particular, assigning to ϕ the same value as on the fluid side implies $\mu=0$ in view of Eq. (15) and leads to pure source surface modeling. Here, however, a doublet lifting surface is required inside the wing and a doublet lift carry-over surface is required inside the body. (Models using doublet singularities on the thick wing and body surfaces are also possible[22] but have not yet been implemented).

Summarizing the mathematical description of the boundary value problem described herein, the following equations determine singularity strength:

$$\hat{n}\cdot W=0 \quad \text{on wing and body}$$

$$\sigma=0, \quad \Delta p_2=0 \quad \text{on free sheet and near wake}$$

$$\Delta\zeta\cdot\hat{\ell}=0 \quad \text{on wing edges (Kutta condition)}$$

$$\sigma=0 \text{ on far wake, fed sheet, body wake, carry-over sheet (24)}$$

Free and fed sheet geometry are then determined by

$$\hat{n}\cdot W_A=0 \quad \text{free sheet}$$

$$\hat{\ell}\times\Delta F=0 \quad \text{fed sheet} \qquad (25)$$

Numerical Procedure

Solution of the above boundary value problem via Eq. (12) is accomplished with the basic panel method of Ref. 23. The method proceeds by dividing the boundary surface into networks. A network is defined as a smooth portion of the boundary which has subsequently been divided into panels and on which source and/or doublet splines have been defined accompanied by properly posed boundary conditions. The networks are assumed to be logically independent in that each network contributes as many equations as unknowns to the overall boundary value problem, hence networks can be added or dropped without total reformulation of the problem. Essential features of the computational scheme are summarized below.

1) Geometry input for a network consists of a rectangular array of corner point coordinates. The portion of the surface lying between four adjacent corner points is approximated by an analytically defined panel.

2) Discrete values of singularity strength are assigned to certain standard points on each network. These values are interpolated by source and doublet splines which on each panel are assumed to be defined by linear and quadratic distributions, respectively.

3) Certain standard points on each network are assigned as control points at which boundary conditions are applied. These points include panel center points as well as edge abutment points in the case of doublet networks. The latter serves to impose standard aerodynamic edge conditions automatically (for example, the Kutta condition, zero potential jump at thin edges, and continuity of singularity strength across abutting networks).

4) The induced potential and velocity integrals of Eq. (12) (influence coefficients) are all evaluated in closed form, although standard far field expansions are employed when the control point is sufficiently distant from the influencing panel.

Figure 2 displays the location of discrete singularity parameters and control points for various network types. These locations are selected to achieve singularity spline stability with respect to the type of boundary conditions applied at the control points.[24] Figure 3 shows a typical thin-wing/body configuration paneling and Fig. 4 shows the same configuration disassembled into networks. Control points located at the junction of two doublet networks (or at the junction of one network with empty space) are assigned to match singularity strength across the junction. If only one control point exists, doublet value is matched. If there are two opposing control points the component of vorticity along the junction is also matched. Control points at panel centers have the boundary conditions prescribed earlier in this section.

In Fig. 5 we display free and fed sheet kinematics. The fed sheet size and position in each x cut are changed by varying the scale parameters λ and ν, the parameter λ scaling the whole vortex system. The free sheet shape is changed by varying the panel orientation angles θ_i, keeping the relative lengths ℓ_i fixed. Note that the vortex system geometry has as many degrees of freedom as constraint Eqs. (25).

Let us now denote all geometry degrees of freedom by the vector Θ and all singularity parameters by Λ. Let us also denote the equation set Eqs. (24) by

$$F(\Lambda,\Theta)=0 \qquad (26)$$

and the equation set Eqs. (25) by

$$G(\Lambda,\Theta)=0 \qquad (27)$$

These equations are solved iteratively by Newton's method

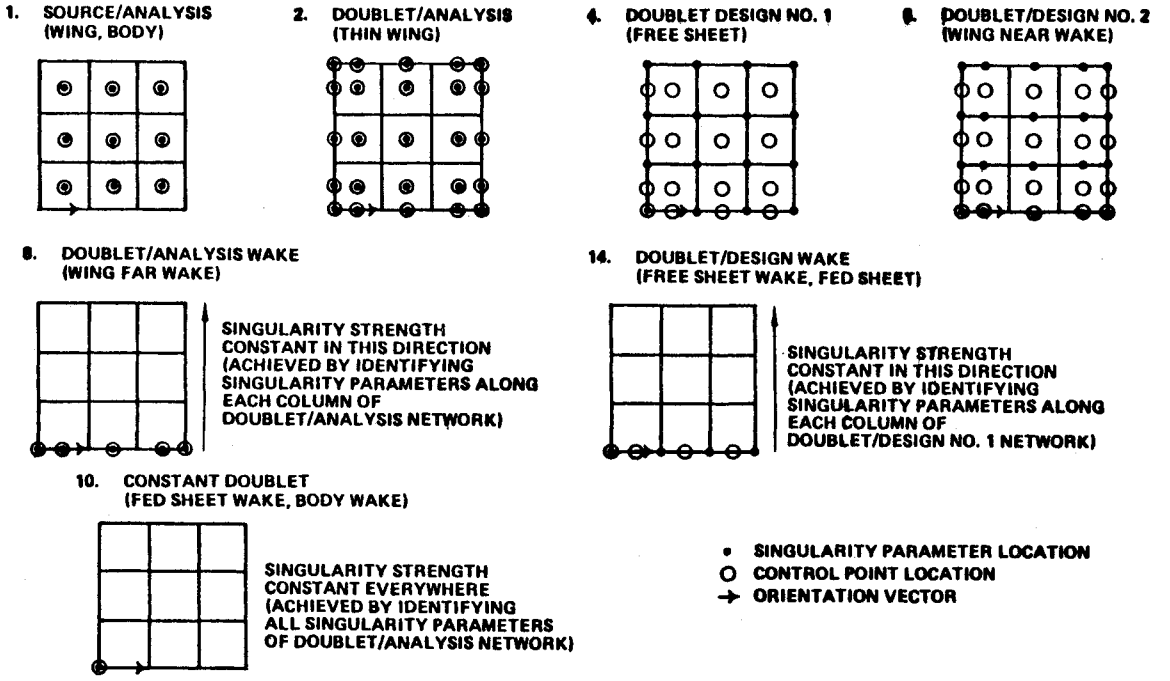

Fig. 2 Location of discrete singularity parameters and control points for various network types.

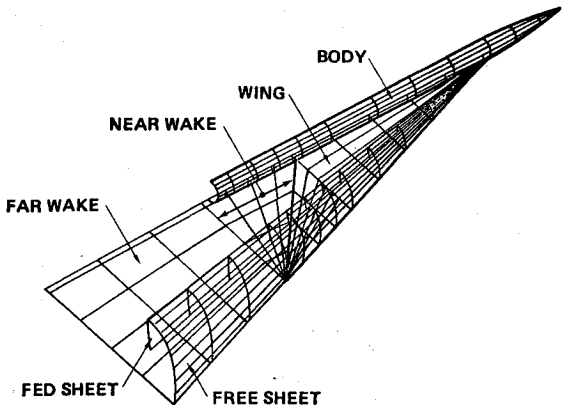

Fig. 3 Panel model.

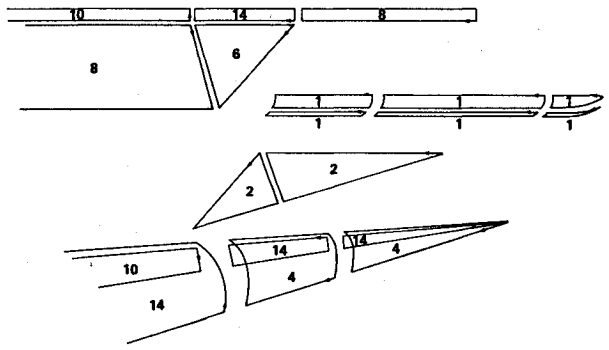

Fig. 4 Networks comprising panel model.

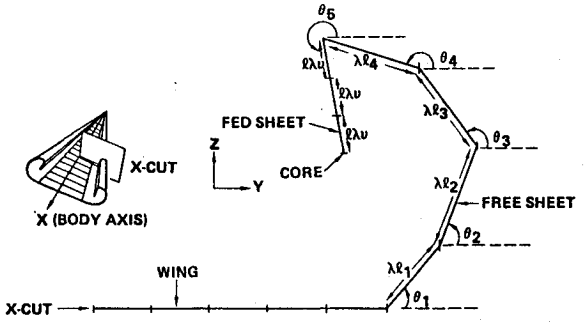

Fig. 5 Free/fed sheet kinematics.

with controlled step size, i.e.,

$$\begin{pmatrix} \frac{\partial F}{\partial \Lambda} & \frac{\partial F}{\partial \Theta} \\ \frac{\partial G}{\partial \Lambda} & \frac{\partial G}{\partial \Theta} \end{pmatrix} \begin{pmatrix} \Delta\Lambda \\ \Delta\Theta \end{pmatrix} = -\rho \begin{pmatrix} F \\ G \end{pmatrix} \tag{28}$$

where ρ is a positive number less than 1 which is chosen small enough to ensure a decrease in the norms of F and G. Note that the Jacobian matrix on the left requires differentiation of the panel influence coefficients with respect to changes in geometry.

III. Recent Advances

Improved Panel Numerics

Equation (13) shows that a discontinuity in doublet strength produces a line vortex of strength equal to the discontinuity. The velocity flowfield induced by such a vortex has a singularity proportional to the vortex strength and inversely proportional to the distance from the vortex. Moreover, the sensitivity to a change in vortex position [appearing in the Jacobian of Eq. (28)] has a singularity inversely proportional to the square of the distance to the vortex. It is clear that if a control point is sufficiently close to such a vortex, the linearization implicit in Eq. (28) will be valid for small $\Delta\Theta$ only, prolonging convergence. Fortunately, the vortex core in our model tends to stay a large distance (relative to its strength) away from wing and free sheet control points. However, our original panel discretization introduced unintentional line vortices which were of small strength but which could be relatively close to wing and free sheet control points. These line vortices arose for two reasons. First, flat panels were generally used for efficiency reasons. These panels were the plane quadrilaterals formed by projecting the straight line segments joining the four corner points onto the plane passing through the midpoints of these line segments. This meant that gaps in geometry would be present at edges of panels belonging to networks where the corner points did not all lie in a plane, leading to ring vortices around each panel. Second, our locally quadratic doublet distribution on each panel was defined by fitting a quadratic function to singularity parameters in an immediate neighborhood. Since each panel used different singularity parameters, continuity of doublet strength across panel edges could not be enforced, and this again led to line vortices. Even on fixed portions of the geometry these vortices created problems because the boundary condition at a panel center control point close to a discontinuity in doublet strength occasionally would attempt to suppress the singularity produced by this discontinuity, i.e., interact with the doublet spline to create greater continuity, rather than control finite flow in the appropriate manner.

In order to alleviate this problem we have implemented the hyperboloidal panels of Morino[25] along with a continuous doublet spline. The hyperboloidal panel H interpolating four corner points Q_1, Q_2, Q_3, Q_4 is defined as the point set

$$H = \{ Q(s,t): \quad Q(s,t) = Q_0 + Q_s s + Q_t t + Q_{st} st;\ s \epsilon [-1,1],\ t \epsilon [-1,1] \} \tag{29}$$

where

$$Q_0 = \tfrac{1}{4}(Q_1 + Q_2 + Q_3 + Q_4) \quad Q_s = \tfrac{1}{4}(Q_1 - Q_2 - Q_3 + Q_4)$$

$$Q_t = \tfrac{1}{4}(Q_1 + Q_2 - Q_3 - Q_4) \quad Q_{st} = \tfrac{1}{4}(Q_1 - Q_2 + Q_3 - Q_4)$$

The panel H is depicted in Fig. 6. Note that H contains the straight line segments joining the edge midpoints Q_5, Q_6, Q_7 and Q_8, the same as the flat panel, and hence H is also only a first order accurate approximation to the true surface. However H also contains the straight lines joining the corner points Q_1, Q_2, Q_3, Q_4 and so it abuts adjacent panels exactly leaving no gaps.

Doublet strength on H is defined parametrically in terms of nine doublet values μ_i at the points Q_i by the formula

$$\mu(s,t) = \mu_1[\tfrac{1}{4}st(1+s)(1+t)] + \mu_2[-\tfrac{1}{4}st(1-s)(1+t)]$$
$$+ \mu_3[\tfrac{1}{4}st(1-s)(1-t)] + \mu_4[-\tfrac{1}{4}st(1+s)(1-t)]$$
$$+ \mu_5[\tfrac{1}{2}t(1+t)(1-s^2)] + \mu_6[-\tfrac{1}{2}s(1-s)(1-t^2)]$$
$$+ \mu_7[-\tfrac{1}{2}(1-t)(1-s^2)] + \mu_8[\tfrac{1}{2}s(1+s)(1-t^2)]$$
$$+ \mu_9[(1-s^2)(1-t^2)] \tag{30}$$

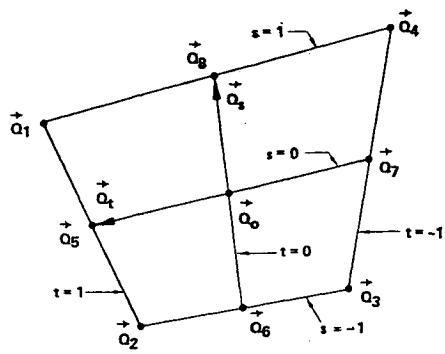

Fig. 6 Hyperboloidal panel.

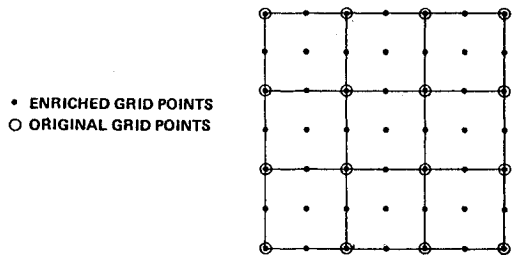

Fig. 7 Enriched grid.

Note that along each of the line segments displayed in Fig. 6 $\mu(s,t)$ is quadratic and is determined solely by the (three) values of doublet strength at the midpoint and endpoints of the segment. The nine doublet values must, of course, be expressed in terms of the free singularity parameters of the network to which H belongs (Fig. 2). For this purpose we define an enriched set of network grid points (Fig. 7) which includes the original corner points, the panel edge midpoints, and center points. At each of these points doublet strength is obtained by fitting a quadratic function to a sufficient number of neighboring singularity parameters by the method of weighted least squares. For stability the closest singularity parameters are weighted heavily, in particular, doublet strength at an enriched grid point coinciding with a singularity parameter point is simply set equal to the value of that parameter. For enriched grid points along network edges the corresponding doublet values are allowed to depend only on singularity parameters located on that edge, and for this purpose a least squares fit based on arc length along the edge is used.

It is clear from the above construction that doublet strength will be continuous across panel edges in the interior of each network. At network junctions doublet strength can also be made continuous so long as the corner points and edge singularity parameter locations coincide. This is the case in Fig. 4 except for the wing/free sheet junction. (Modification of some of the edge singularity parameter locations for both doublet/design networks could eventually lead to precise continuity everywhere.)

Calculation of the influence coefficients for the above formulation is accomplished using Eq. (13), where the last term on the right may now be discarded entirely except for the fed sheet terminated edge. Evaluation of the remaining integrals is facilitated by an expansion which is similar to the curved panel expansion of Ref. 23, but which does not require the small curvature assumption. Rewriting the second integral on the right of Eq. (13) in terms of the parameters s and t we obtain

$$\iint_H \zeta(Q)\times\tilde{\nabla}_Q\left(\frac{1}{4\pi R}\right)dS_Q=\frac{\beta^2}{4\pi}\int_{-1}^{1}\int_{-1}^{1}\frac{1}{R^3}\times\left[\frac{\partial\mu}{\partial s}(a_t\times a_{t0})-\frac{\partial\mu}{\partial t}(a_s\times a_{s0})\right]dsdt \tag{31}$$

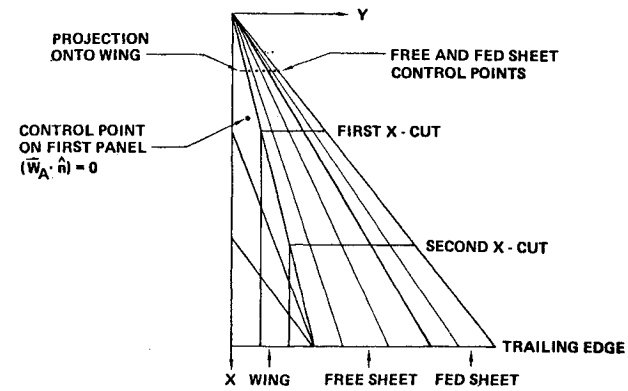

Fig. 8 Streamwise paneled delta wing with unwrapped free and fed sheets.

where

$$R=R_0-Q_s s-Q_t t-Q_{st}st,\quad R_0=P-Q$$

$$a_s=Q_s+Q_{st}t,\quad a_t=Q_t+Q_{st}s,$$

$$a_{s0}=R_0-Q_t t,\quad a_{t0}=R_0-Q_s s$$

The term in square brackets on the right of Eq. (31) is simply a polynomial, but the integration cannot be performed in closed form since R is a quartic polynomial in s and t. However, we can approximate R as follows. Let (s^*, t^*) minimize R on $[-1,1]\times[-1,1]$, so that $Q(s^*, t^*)$ is a closest point on H to P in the compressible norm. Let $R^*(s,t)$ be the quadratic part of R at the point (s^*,t^*), i.e.,

$$R^*(s,t)=(R_0-Q_s s^*-Q_t t^*-Q_{st}s^*t^*)-Q_s(s-s^*)-Q_t(t-t^*) \tag{32}$$

Then $(R^*/R)^3$ is continuous in s and t and may be approximated to any accuracy by a polynomial $T(s,t)$. Upon substitution of the approximation

$$1/R^3\approx[T(s,t)/R^{*3}] \tag{33}$$

into the right side of Eq. (31) the integration may be performed in closed form.

Evaluation of the surface vortex integral using the above procedure is quite accurate but rather expensive. Hence, a somewhat simpler approximation was developed for use in the intermediate field, i.e., when the field point is a modest distance away from the panel but not sufficiently distant that a far field expansion converges. For this approximation the flat panel is used again along with the quadratic doublet distribution [based on surface coordinates (ξ,η)]:

$$\mu(\xi,\eta)=\mu_0+\mu_\xi\xi+\mu_\eta\eta+\tfrac{1}{2}\mu_{\xi\xi}\xi^2+\mu_{\xi\eta}\xi\eta+\tfrac{1}{2}\mu_{\eta\eta}\eta^2 \tag{34}$$

Here the coefficients are obtained by expanding Eq. (30) in a Taylor series about the panel center. (Note that the doublet strength obtained from Eq. (34) then agrees identically with that of Eq. (30) along the lines $s=0$ and $t=0$.) We found that this approximation agreed well with the more exact calcualtion above—even for the field point at the panel center, hence, we decided to use it exclusively in the near field. While it would then seem that we are back to the flat panel/quadratic doublet distribution at least for the purpose of calculating influence coefficients, it is important to realize that the underlying panel shape and doublet distribution are given by Eqs. (29) and (30), respectively. With the old method it was impossible to ignore the line vortex term on the right side of Eq. (13) since the doublet strength could not be deduced from knowledge of the vorticity vector alone.

Leat Squares Geometry Update Procedures

In Fig. 8 we show a streamwise paneled delta wing with unwrapped free and fed sheets. The control point on the first wing panel is displayed. The control point on the first row of panels on the free and fed sheets are also displayed along with their projection onto the wing. Since the first wing control point is so far from the apex, flow through the wing near the apex is not prevented and, consequently, the free and fed sheet control points in the first row encounter a somewhat different environment than those in subsequent rows. To satisfy the boundary condition at these control points the whole vortex system near the apex is required to move substantially inboard causing errors in wing pressures at the first wing control point. Obviously with such a paneling one cannot be too concerned with flow details at the apex anyway. In the past, however, the flow anomaly there destroyed convergence everywhere even though the flow is better behaved further aft on the wing.

The problem was twofold. First, all equations of the set Eqs. (25) were required to be satisfied exactly. Because huge local anomalies in vortex sheet shape were required the singularities themselves got involved heavily in solving Eq. (25) with consequential loss of stability. Second, our update procedure was such that local anomalies in sheet shape could propagate to other areas of the sheet. In other words, the procedure itself was not fully stable. The basic reason has to do with the fact that for both the flat and hyperboloidal panels the surface normal at the panel center remains unchanged when the four panel corner points are alternatingly perturbed equal distances above and below the average plane. For illustration purposes assume the free sheet lies in a plane as shown in Fig. 9. The average mass flux vectors at the panel centers are depicted with arrows and are assumed to lie in the plane as well, except for the mass flux vector at the center of the first panel which, because of a flow anomaly, is assumed to be substantially out of plane. We assume that all corner points except for those in the inboard column (which are attached to the wing) may be perturbed in a direction normal to the surface (i.e., plane) and we also assume that the mass flux vector W at each panel center is little altered by such a perturbation. The boundary condition $(W\cdot\hat{n})=0$ is already satisfied on all panels except the first, where a perturbation of corner point 3 by a large distance h is required to modify the panel center normal so that $(W\cdot\hat{n})=0$. A perturbation of corner point 4 by $-h$ is required to maintain the boundary condition on panel 2, and so on down the line. Thus the effect of the flow anomaly on panel 1 is propagated to the whole free sheet with the consequence that all the quadrilateral panels become considerably twisted.

Probably the simplest method of damping this instability whenever it arises is to limit excessive panel twist. A measure of panel twist is the function

$$K=(n\cdot Q_{st})/(n\cdot n)^{1/4} \tag{35}$$

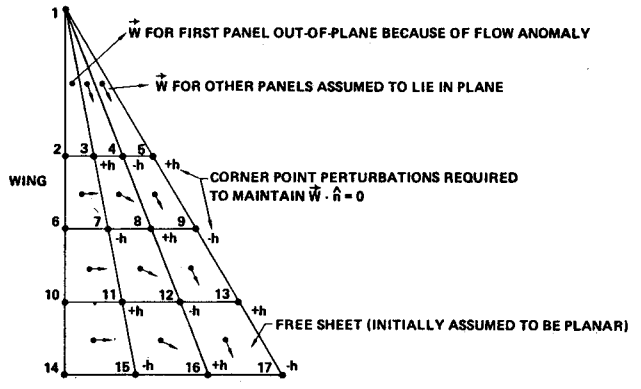

Fig. 9 Geometry update instability.

where $n=Q_s\times Q_t$. The condition that all free sheet panels be untwisted (flat) is

$$K(\Theta)=0 \tag{36}$$

using the notation of Eqs. (26) and (27). Equation (36) combined with Eqs. (26) and (27) creates an overdetermined system of equations for Λ and Θ. We view Eq. (26) as an equation which defines Λ as a function of Θ, i.e.,

$$F(\Lambda,\Theta)=0\Rightarrow\Lambda=f(\Theta) \tag{37}$$

Substituting Eq. (37) into Eq. (27) we then have two competing equation sets for determining Θ, i.e.,

$$G[f(\Theta),\Theta]=0 \text{ and } K(\Theta)=0 \tag{38}$$

This system is solved in a least square sense after suitable normalization to account for dimensional differences as well as desired weighting. Obviously, we do not wish to weight the penalty Eq. (36) heavily since, in general, a free sheet made up entirely of untwisted panels cannot be a good approximation to a stream surface. Fortunately, a small weight is all that is required. The instabilities produced by a local flow anomaly are severe enough that a very small penalty on panel twist forces relaxation of the boundary condition causing the local anomaly.

The procedure for solving the overdetermined equation set is iterative as before. At the beginning of an iteration Eq. (26) is solved for Λ as a function of the current Θ using Newton's method with controlled step size, i.e.,

$$\frac{\partial F}{\partial\Lambda}\Delta\Lambda=-\rho F \tag{39}$$

Upon obtaining convergence a new estimate for Θ is calculated by solving the equation

$$\begin{pmatrix}\dfrac{\partial G}{\partial\Lambda} & \dfrac{\partial f}{\partial\Theta}+\dfrac{\partial G}{\partial\Theta}\\ \dfrac{\partial K}{\partial\Theta}\end{pmatrix}(\Delta\Theta)=-\rho\begin{pmatrix}G\\K\end{pmatrix} \tag{40}$$

in a least-square sense, where the Jacobian on the left is evaluated at the point $\Lambda=f(\Theta)$ as determined from Eq. (39) and $\partial f/\partial\Theta$ is calculated from

$$\frac{\partial F}{\partial\Theta}\frac{\partial f}{\partial\Theta}+\frac{\partial F}{\partial\Theta}=0 \tag{41}$$

We assume here that G and K have been normalized appropriately.

IV. Numerical Verification

In this section we present cases generated by the computer program implementing the current method. The purpose of these cases is to display those numerical characteristics of the method which are important for establishing confidence in the computed results.

Effect of Wing Panel Density

In Fig. 10 we show the effect of wing panel density on vortex system geometry, wing pressures, and forces and moments. The primary effect is associated with spanwise density and so in Fig. 10a we show conically paneled wings having 6 and 12 panels spanwise. In both panelings the spacing is nonuniform with a concentration of panels where they are obviously most required, namely outboard under the vortex. The effect of an increase in density is to move the vortex system slightly outboard as shown in Fig. 10b, and the

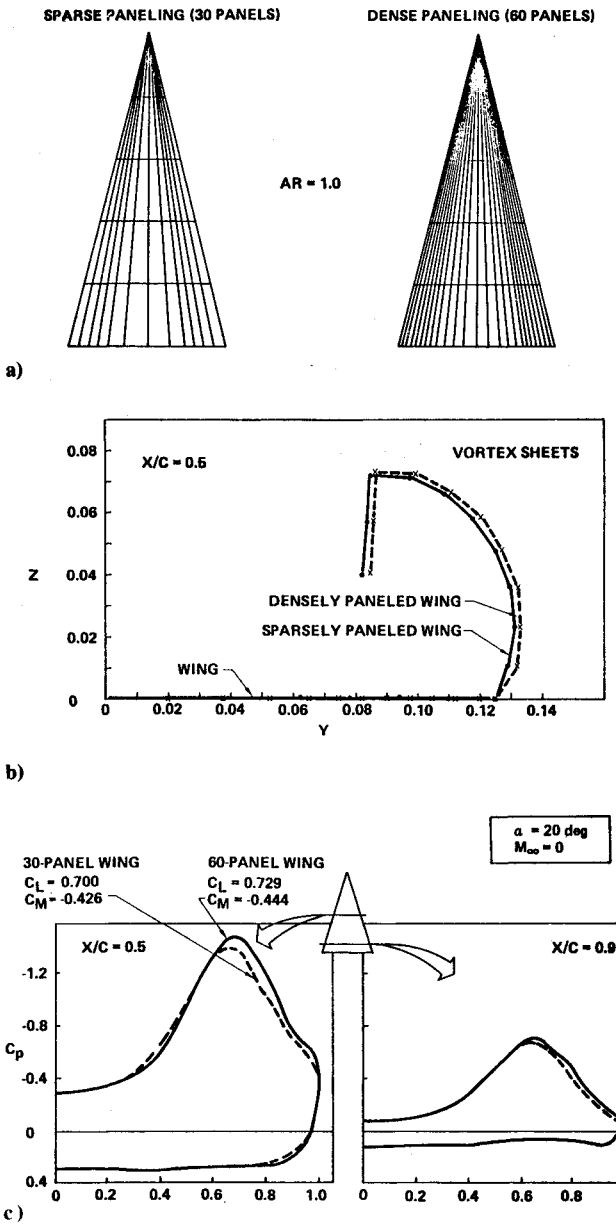

Fig. 10 Effect of wing panel density: a) wing paneling, b) vortex system geometry, c) wing pressure.

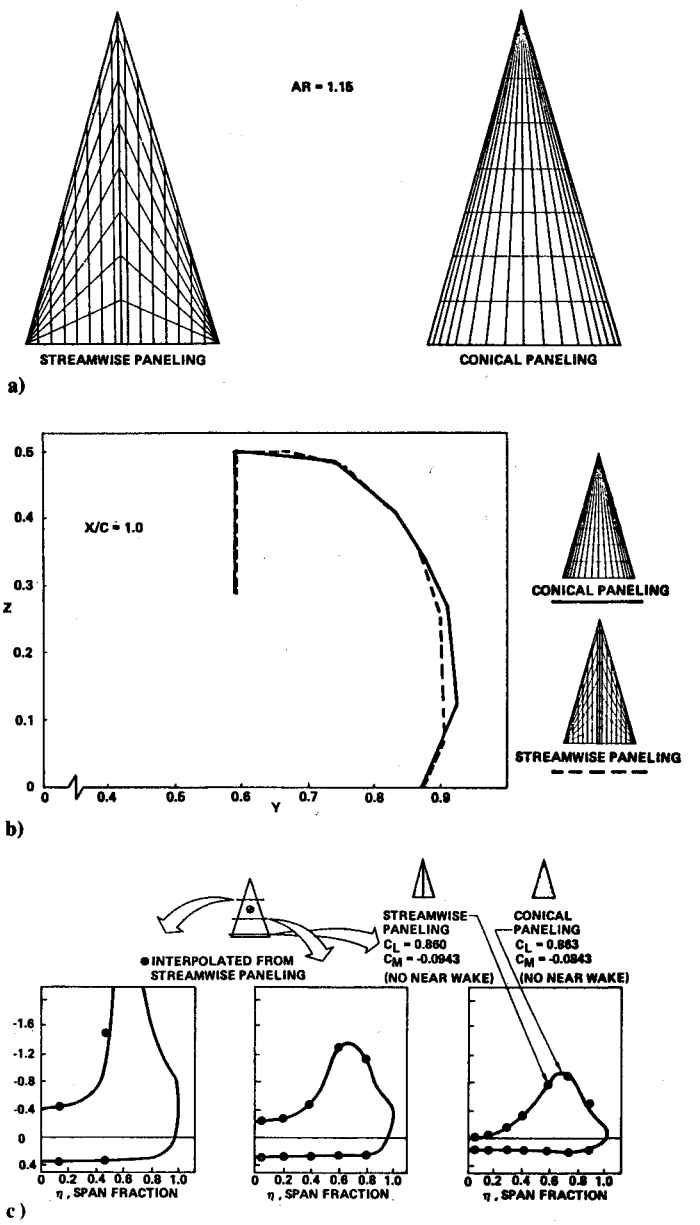

Fig. 11 Effect of wing panel layout: a) wing paneling, b) vortex sheet geometry, c) wing pressures.

consequence is somewhat higher pressures on the upper surface outboard of the votex core as shown in Fig. 10c. The lift coefficient is correspondingly higher (see also Fig. 18b). We have run greater spanwise densities but the incremental effect is negligible compared with that shown in Fig. 10.

Effect of Wing Panel Layout

In Fig. 11 we compare computed results for the two panel layouts usually employed on delta wings, i.e., streamwise and conical. Both layouts have 64 panels. The least square procedure described in Sec. III was required to obtain convergence for the streamwise paneling. Wing pressures and force and moment coeffficients are displayed in Fig. 11b. Pressures for the streamwise paneling have been interpolated to the control point locations of the conical paneling for comparison purposes. The two cases were run about a year apart and in the intervening time a study on initial sheet shape was made, hence, the free sheets have somewhat different panel spacing. However, comparisons of pressure and force data still show excellent agreement.

Effect of Vortex Sheet Rollup

The cornerstone of the current method is, of course, Smith's device for terminating the free sheet rollup; namely, the use of fed sheet whose position and size are determined by the same overall condition that would be applicable to an infintely rolled up free sheet. The point at which the free sheet rollup should be terminated by a fed sheet depends upon the sensitivity of wing pressures to further rollup. This matter has been investigated in detail by Smith[6] under the assumption of conical flow, and the standard amount of rollup employed by the current method is based on his results. To verify the application to fully three-dimensional flow delta wings of aspect ratio 0.25, 1.0 and 2.0 have been analyzed with an additional 180 deg of rollup. Results at $\mathcal{R} = 0.25$ are shown in Fig. 12 and indicate a slight increase in lift (4%) with increased rollup. The effect of rollup is much less at the higher aspect ratios (1% at $\mathcal{R} = 1.0$ and less than 0.5% at $\mathcal{R} = 2.0$). Results for $\mathcal{R} = 2.0$ are shown in Fig. 13. We have generally concluded that the standard rollup is adequate for all models. The slight improvements available at low aspect ratios do not seem to warrant the added complexity and expense of additional rollup.

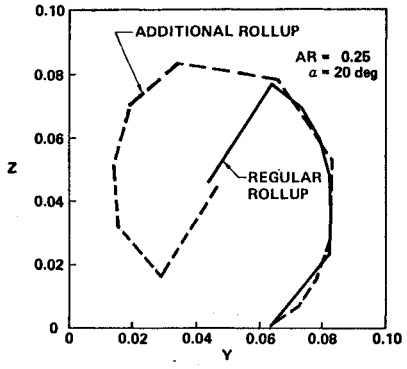

a)

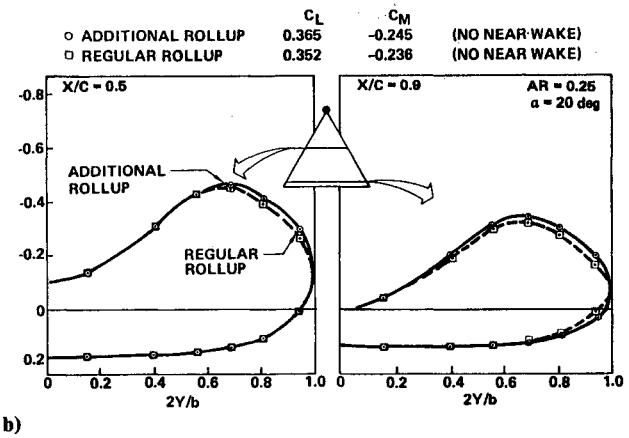

b)

Fig. 12 $\mathcal{R}=0.25$ delta wing with additional free sheet rollup: a) vortex sheet geometry, b) wing pressures.

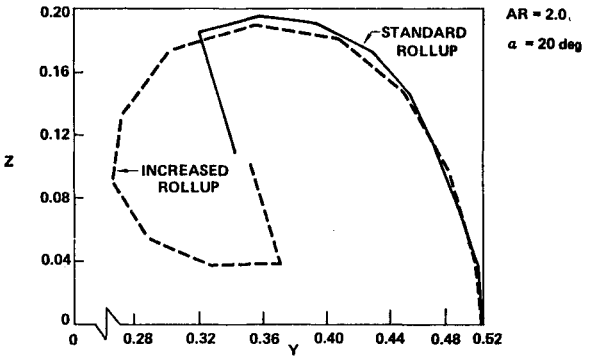

a)

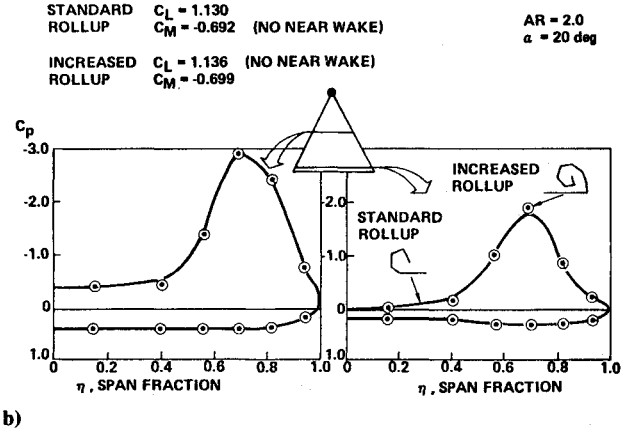

b)

Fig. 13 $\mathcal{R}=2.0$ delta wing with additional free sheet rollup: a) vortex system geometry, b) wing pressures.

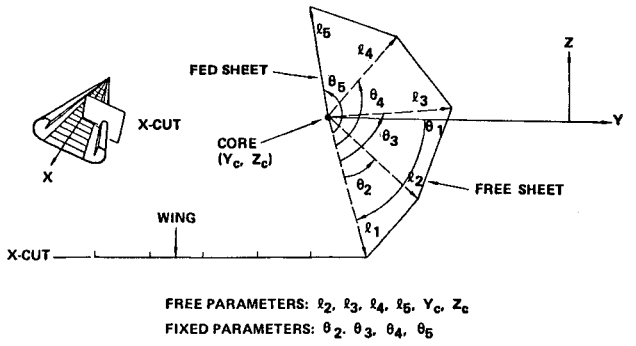

Fig. 14 Smith's free/fed sheet kinematics.

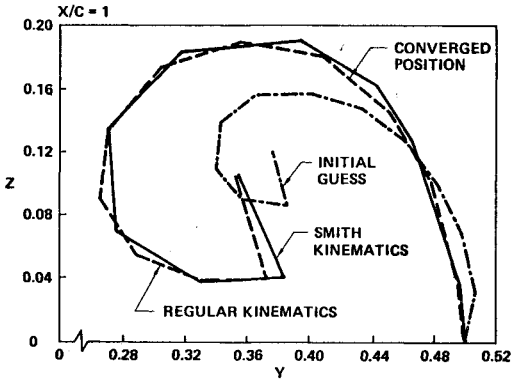

a)

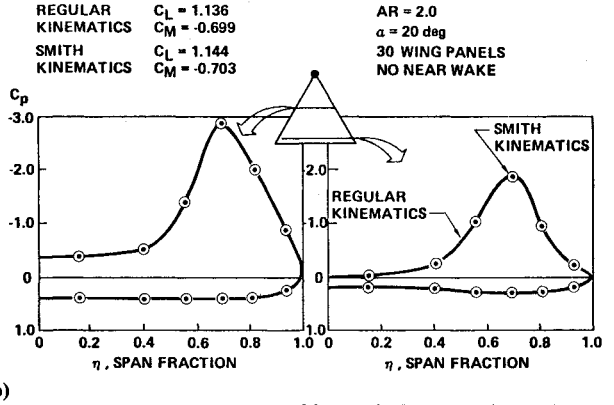

b)

Fig. 15 Effect of vortex system kinematical assumptions: a) vortex system geometry, b) wing pressures.

Effect of Vortex System Kinematics

Our standard vortex system kinematics shown in Fig. 5 is, of course, only one for many possibilities. A good alternative is the kinematics of Smith[6] shown in Fig. 14. Here, in contrast to our standard kinematics, angles are fixed and lengths are chosen as free parameters. Smith's kinematics have also been coded into the computer program implementing the current method with results typified in Fig. 15. Comparisons have been made for small and large free sheet rollups, for core locations inboard and in the vicinity of the leading edge, and for wings of small and large aspect ratio, all with similarly close results. If any difference has been noticed, it is that Smith's kinematics seems to converge somewhat faster than our standard kinematics with corresponding savings in run cost.

Kutta Condition

In Sec. II we described the manner in which the current method enforces the Kutta condition at a wing edge. We pointed out that the equation formally assigned as the Kutta condition is actually a restriction on singularity strength

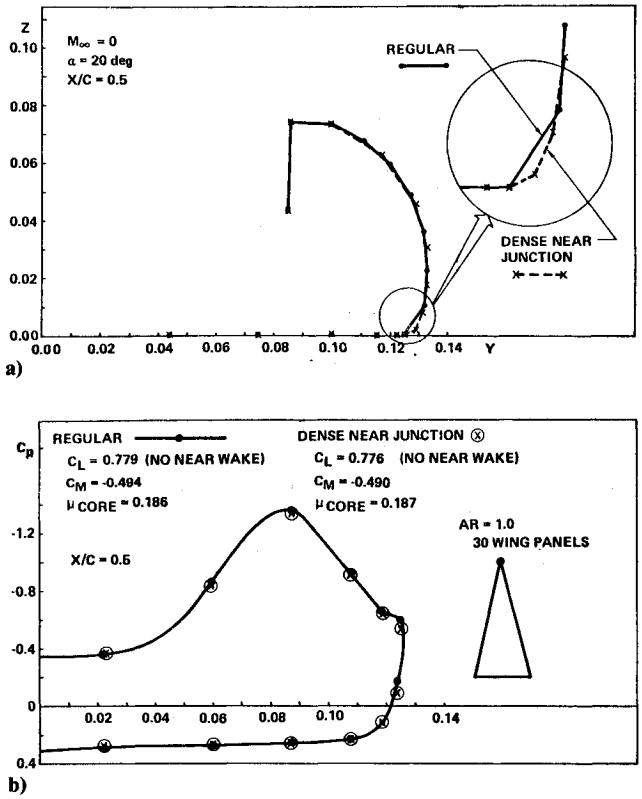

Fig. 16 Kutta condition: a) wing/vortex system geometry, b) wing pressure.

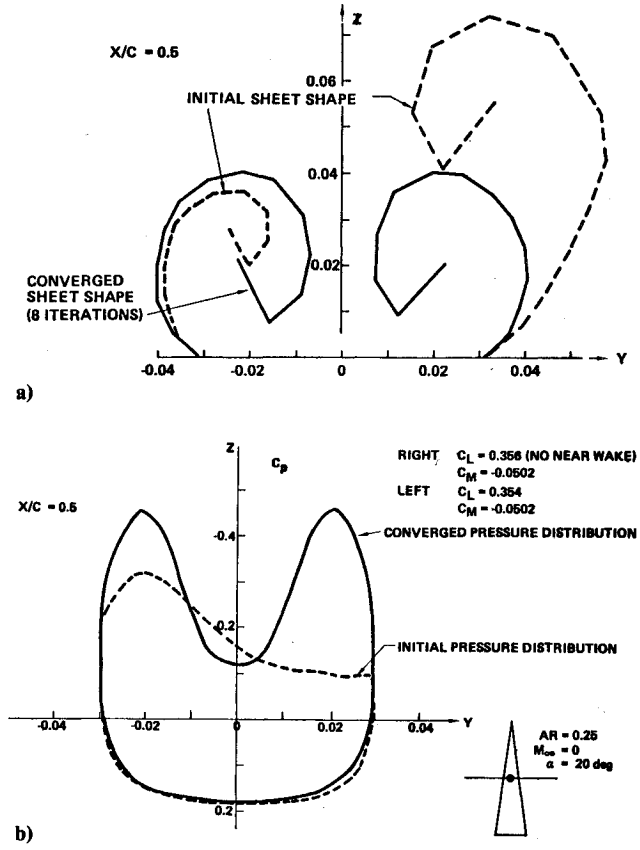

Fig. 17 Asymmetric initial sheet shape: a) vortex system geometry, b) wing pressure.

rather than the flow, namely, that the component of vorticity parallel to the wing edge be continuous onto the vortex sheet. This condition when combined with the standard flow boundary conditions assigned to the interior of the wing and free sheet then creates those properties at the edge commonly associated with the Kutta condition, i.e., finite flow, zero pressure jump, etc. We also pointed out that finite flow requires continuity of all components of the vorticity vector across the edge, which can only happen when the wing and free sheet adjoin smoothly. This fact seems somewhat inconsistent with out converged vortex system geometry (e.g., Fig. 10b) which usually displays a large discontinuity in surface shape at the wing-sheet junction. However, the discontinuity in surface slope is no different qualitatively than any other on the vortex system and can be reduced (and in the limit eliminated) by dense paneling. In Fig. 16 we show the effects of finer vortex sheet paneling at the wing junction and note that the discontinity in surface slope at the junction is reduced considerably. To reduce the discontinuity in surface slope in the neighborhood of the junction to the point where the surface would appear smooth to plotting accuracy would require extremely fine paneling at enormous expense. Fortunately, such paneling is not required unless precise details of the flow in the neighborhood of the junction are required for reasons other than establishing the Kutta condition. This is because the global effects of the Kutta condition are already accounted for by our particular implementation. We note from Fig. 16b that dense free sheet paneling near the junction has little effect on lift and moment coefficients, vortex core position and strength, and pressure distributions except at the junction.

Effect of Initial Free and Fed Sheet Shape

Aside from free sheet rollup and panel density the initial guess of sheet shape and size has little bearing on converged results (assuming, of course, the boundary value problem has a unique solution) although convergence itself will be affected. Figure 17 illustrates this point. In Fig. 17b we display a converged pressure distribution and force and moment coefficients for an aspect ratio 0.25 delta wing at 20 deg angle of attack and no yaw. The initial sheet shape is considerably asymmetric, however, the converged sheet shape is quite symmetric given the fact that rollup on left and right sides are slightly different. More importantly, the pressure distribution and force and moment coefficients are very nearly symmetric. Note the close agreement in values with the solution employing a plane of symmetry in Fig. 12.

V. Comparisons with Experiment and Other Theories

In this section we present computed results for the purpose of examining the validity of the theoretical model described in Sec. II. Many such results have been reported previously.[15,18,26] Particular note should be taken of Ref. 26 in which the capabilities of the method in analyzing cambered wings are illustrated. Results presented here will be those that are primarily new in nature.

Lift Coefficient as a Function of Aspect Ratio

In Sec. I we discussed the problem associated with the method overpredicting lift coefficient at high aspect ratio, and how this problem was eliminated by use of the more accurate near wake (type 6, Fig. 2) at the wing trailing edge. Resolution of the problem is shown in Fig. 18. The dashed line in Fig. 18b shows the lift coefficients calculated using a far wake (type 8) only. (Results using 60 wing panels would be somewhat higher at the high aspect ratios.) Insertion of near wake (shown in Fig. 18a) yields lift coefficients which are in substantially better agreement with the suction analogy and experiment.[2,27-30] These lift coefficients are based on a near wake of 0.5 root wing chord in length divided into three rows of panels. (Note that the free/fed sheet vortex system must extend to the end of the near wake.) In order to study the sensitivity of the wing pressures to near wake length, two

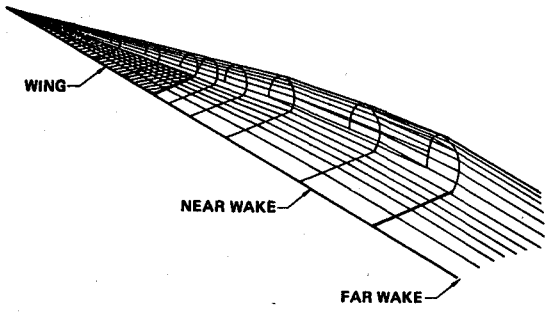

a)

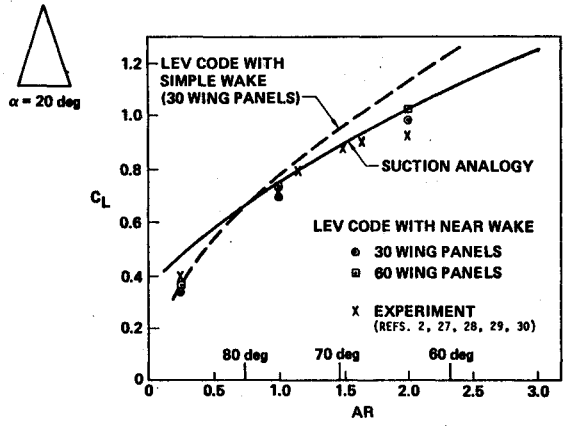

b)

Fig. 18 Delta wings with near wake: a) wing, vortex system, and wake geometry, b) variation of lift with aspect ratio.

additional near wakes were tested. One was 1.5 root chords long and made up of 5 rows of panels (Fig. 18a). The other was 0.1 root chords and made up of 2 rows of panels. Wing pressures for all three wakes were practically identical indicating, as stated in Sec. II, that the primary function of this wake is to establish the proper wing trailing edge Kutta condition.

The question of lack of agreement between the suction analogy, experiment, and the current method at very low (<0.5) or high (>1.5) aspect ratios still remains. Examination of the results shows that for a very low (0.25) aspect ratio the experimental data lies nearly halfway between the results of the current method (low) and suction analogy (high). However, analysis of the experimental data[29] reveals that at the 20 deg angle of attack shown, an asymmetrical vortex has developed in the real flow. This is indicated by the rolling moment at zero yaw that developed at angles of attack greater than about 16 deg. The theoretical models assume symmetrical vortices. Luckring (NASA LRC) has computed solutions at several angles of attack using the current method. His results presented in Fig. 19 show excellent agreement between the method and experimental data at the lower angles of attack. Beginning with the 15 deg angle of attack the results start to deviate from the experimental data. Since this is approximately where the leading edge vortices become asymmetrical while the theory vortices remain symmetric, it is conceivable that this phenomenon could somehow be responsible for the deviation.

Suction analogy results are also shown in Fig. 19. These results also deviate from experiment at the higher angles of attack but in the opposite manner. Polhamus (NASA LRC) has suggested that the suction analogy may be high for these cases because the analogy assumes complete reattachment of the leading edge vortex and, therefore, complete recovery of the suction force. As previously shown in Fig. 12 for low aspect ratio deltas at high angles of attack, the size of the free sheet which represents the vortex shear surface has become so

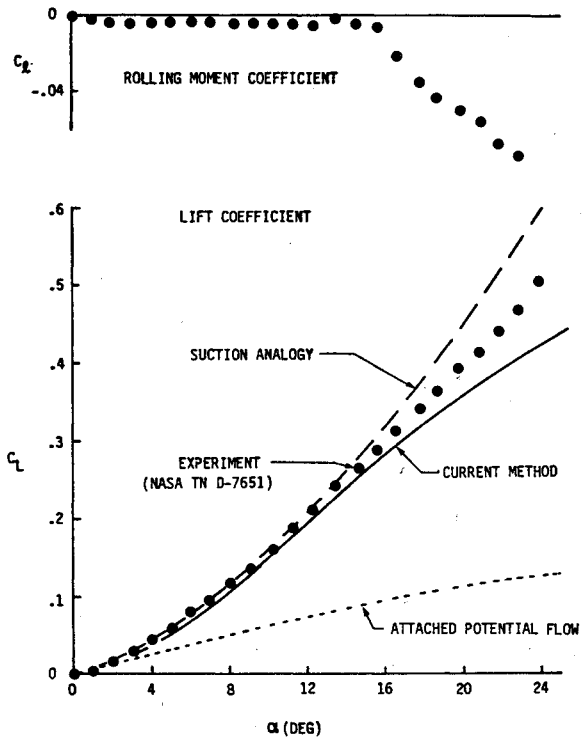

Fig. 19 Aerodynamic characteristics of aspect ratio 0.25 wing.

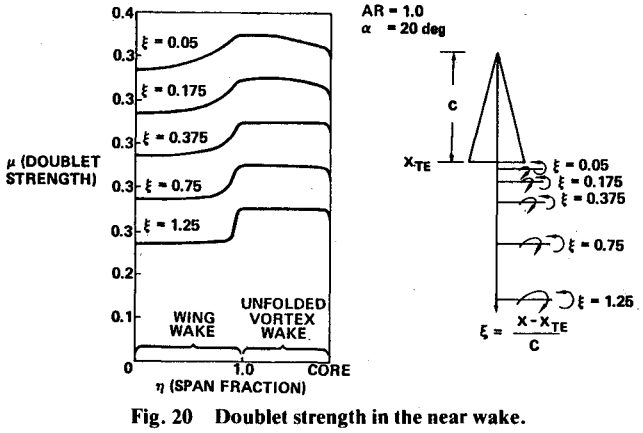

Fig. 20 Doublet strength in the near wake.

large that it may be preventing complete reattachment and, therefore, complete suction recovery.

At the higher aspect ratios, the current method is in good agreement with the suction analogy but both methods predict higher lift coefficients than shown by the experimental data. Examination of the experimental results shows a loss in lift at the higher angles of attack due to vortex bursting. Since neither the current method nor the suction analogy can account for this phenonema, exact correlation with experimental data is not possible.

Wake Vorticity Rollup

An interesting property of the solution produced by the current method was discovered with the use of the near wake. In real flow over a delta wing with a leading edge vortex, the wake behind the wing will roll up into a vortex rotating counter to that of the leading edge vortex. This phenomenon has been known for some years and was clearly evident in the experimental measurements presented by Hummel[31] at a recent AGARD symposium on high angle of attack flows. Examination of the doublet strength in the near wake and connecting free sheet clearly reflects this behavior. Doublet strength is plotted vs span fraction on the wake and unrolled

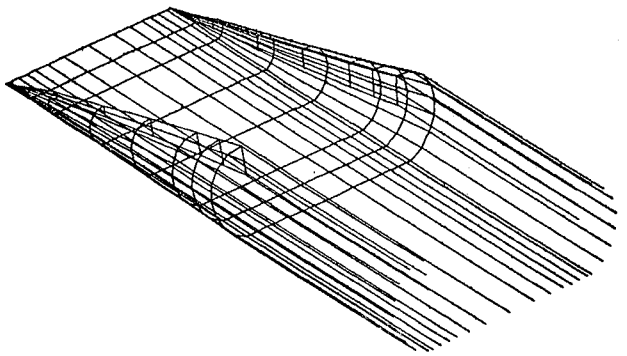

a) Wing and vortex system geometry

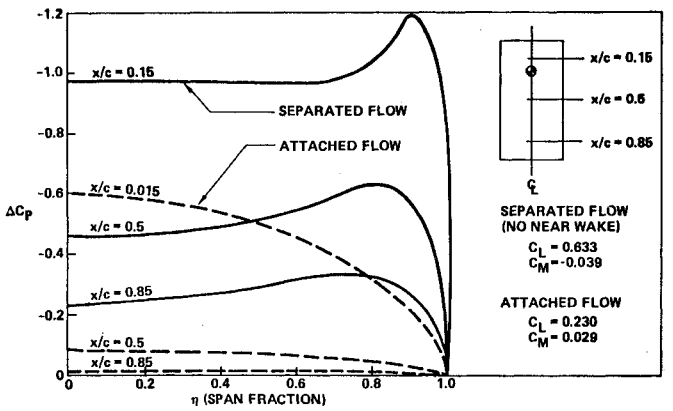

b) Wing pressure distributions (ΔC_p) at $AR = 0.5$

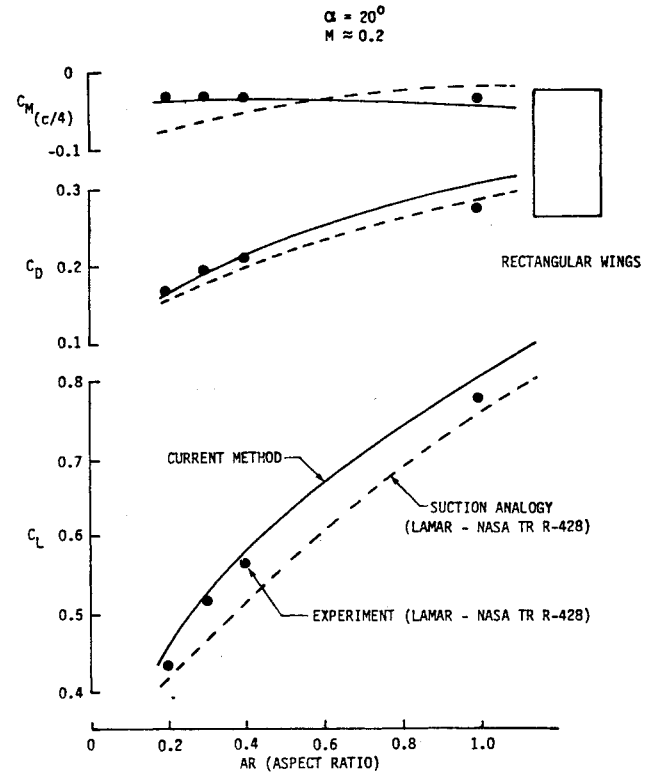

c) Force and moment coefficients

Fig. 21 Rectangular wing with side-edge separation.

free sheet for several cuts behind the delta wing in Fig. 20. Near the trailing edge the doublet strength gradually rises toward the wing tip indicating an outward spanwise vorticity flow in a direction counter to that of the vortex core denoted by the sudden drop of doublet strength (note that vorticity is the gradient of the doublet strength). Moving away from the trailing edge the variation of doublet strength becomes flatter except for the jumps behind the tip and the vortex core. This indicates the concentration of vorticity into two counter rotating vortices just as in the real flow. Presumably it would be possible to replace the whole wake by such counter rotating vortices at about 0.5 root chords behind the wing in order to determine the effect on downstream components of a more complex configuration.

Rectangular Wings

In Fig. 21a we display converged geometry for an aspect ratio 0.5 rectangular wing with separated flow around the side edges. Corresponding pressure distributions ΔC_p are plotted in Fig. 21b along with similar distributions for the same wing in an unseparated condition (which were generated by simply removing the vortex networks). Force and moment coefficients for rectangular wings of varying aspect ratio are shown in Fig. 21c and comparisons with the suction analogy and experiment[32] are good. Convergence for these cases required use of the least squares technique described in Sec. III.

VI. Conclusions

The advances described in this paper clearly improve the usefulness of the current method in the study of separated vortex flow. In addition, the numerical examples set forth in Sec. IV give reasonable assurance that data computed by the method faithfully reflects the underlying flow model. For those cases in which the real flow deviates significantly from the single well formed vortex assumed in the flow model, the method generally tends to fail. Finally, the results accumulated to date show that the flow model itself is representative of the physics in a wide variety of cases.

Acknowledgment

This paper is based on work conducted for Langley Research Center under NASA Contracts NAS1-15169 and NAS1-15272 with additional computing support from the Ames Research Center, and also on work conducted for the Boeing Independent Research and Development Program. The authors wish to thank P. E. Rubbert for his guidance in certain critical areas of the current investigation. The authors would also like to thank J. M. Luckring, and E. C. Polhamus of NASA Langley for applicable data and fruitful discussions.

References

[1] Maskell, E. C., "Some Recent Developments in the Study of Edge Vortices," *Proceedings of 3rd Congress of International Council of Aerospace Sciences, 1962,* Spartan Books, Inc., Washington, 1964, pp. 737-749.

[2] Peckham, D. H., "Low-Speed Wing-Tunnel Tests on a Series of Uncambered Slender Pointed Wings with Sharp Edges," British Aeronautical Research Council, RM 3186, 1961.

[3] Polhamus, E. C., "Predictions of Vortex-Lift Characteristics by a Leading-Edge Suction Analogy," *Journal of Aircraft*, Vol. 8, April 1971, pp. 193-199.

[4] Polhamus, E. C., "A Concept of the Vortex Lift of Sharp-Edge Delta Wings Based on a Leading-Edge-Suction Analogy," NASA TN D-3767, Dec. 1966.

[5] Polhamus, E. C., "Application of the Leading-Edge-Suction Analogy of Vortex Lift to the Drag-Due-to-Lift of Sharp-Edge Delta Wings," NASA TN D-4739, Aug. 1968.

[6] Smith, J.H.B., "Improved Calculations of Leading-Edge Separation from Slender Delta Wings," RAE Tech. Rept. 66070, March 1966.

[7] Mangler, K. W. and Smith, J.H.B., "A Theory of the Flow Past a Slender Delta Wing with Leading-Edge Separation," *Proceedings of the Royal Society*, May 1959.

[8] Nangia, R. K. and Hancock, G. J., "A Theoretical Investigation for Delta Wings with Leading-Edge Separation at Low Speeds," Aeronautical Research Council, ARC CP 1086, 1968.

[9] White, R. P. Jr., "Wing-Vortex Lift at High Angles of Attack," AGARD-CP-204, Sept. 1976.

[10] Kandil, O. A., Mook, D. T., and Nayfeh, A. H., "Nonlinear Prediction of the Aerodynamic Loads on Lifting Surfaces," *Journal of Aircraft*, Vol. 13, Jan. 1976, pp. 22-28.

[11] Rehbach, C., "Etude, Numerique de Nappes Tourbillonaires Issues D Une Ligne de Decollement Pres du Bord d' Attaque," *Recherches Aerospatiales*, 1973-6, 1973, pp. 325-330.

[12] Kandil, O. A., Mook, D. T., and Nayfeh, A. H., "A Numerical Technique for Computing Subsonic Flow Past Three-Dimensional Canard-Wing Configurations with Edge Separations," AIAA Paper 71-1, 1977.

[13] Kandil, O. A., Atta, E. H., and Nayfeh, A. H., "Three Dimensional Steady and Unsteady Asymmetric Flow Past Wings of Arbitrary Planforms," AGARD-CP-227, Sept. 1977.

[14] Weber, J. A., Brune, G. W., Johnson, F. T., Lu, P., and Rubbert, P. E., "Three-Dimensional Solution of Flows over Wings with Leading Edge Vortex Separation," *AIAA Journal*, Vol. 14, 1976, pp. 519-525; also NASA CR 132709 and 132710, April 1975.

[15] Johnson, F. T, Lu, P., Brune, G. W., Weber, J. A., and Rubbert, P. E., "An Improved Method for the Prediction of Completely Three-Dimensional Aerodynamic Load Distributions on Configurations with Leading-Edge Separation," AIAA Paper 76-417, 1976.

[16] Hoeijmakers, H.W.M. and Bennekers, B., "A Computational Method for the Calculation of the Flow about Wings with Leading-Edge Vortices," Paper 25, AGARD-CP-247, Jan. 1979.

[17] Smith, J.H.B., "Inviscid Fluid Models, Based on Rolled-Up Vortex Sheets, for Three-Dimensional Separation at High Reynolds Number," Paper 9, *AGARD Lecture Series No. 94 on Three-Dimensional and Unsteady Separation at High Reynolds Numbers*, Feb. 1978.

[18] Kuhlman, J. M., "Analytical Studies of Separated Vortex Flow on Highly Swept Wings," NASA CR-3022, Nov. 1978.

[19] Brune, G. W. and Rubbert, P. E., "Boundary-Value Problem of Configurations with Compressible Free Vortex Flow," *AIAA Journal*, Vol. 15, Oct. 1977, pp. 1521-1523.

[20] Kellogg, O. D., *Foundations of Potential Theory*, Dover Publishing Company, New York, 1953.

[21] Lamb, H., *Hydrodynamics*, Dover Publishing Company, New York, 1945.

[22] Johnson, F. T., Ehlers, F. E., and Rubbert, P. E., "A Higher Order Panel Method for General Analysis and Design Applications in Subsonic Flows," *Proceedings of the Fifth International Conference on Numerical Methods in Fluid Dynamics*, Enschede, The Netherlands, June 1976.

[23] Johnson, F. T. and Rubbert, P. E., "Advanced Panel-Type Influence Coefficient Methods Applied to Subsonic Flows," AIAA Paper 75-50, Jan. 1975.

[24] Hess, J., Johnson, F. T., and Rubbert, P. E., *Panel Methods Lecture Notebook*, AIAA Short Course on Panel Methods, July 1978, pp. 3-20–3-28.

[25] Morino, L., Chen, L., and Suciu, E O., "Steady and Oscillatory Subsonic and Supersonic Aerodynamics Around Complex Configurations," *AIAA Journal*, Vol. 13, March 1975, pp. 368-374.

[26] Tinoco, E. N. and Yoshihara, H., "Subcritical Drag Minimization for Highly Swept Wings with Leading Edge Vortices," Paper 26, AGARD-CP-247, Jan. 1979.

[27] Wentz, W. H., "Effects of Leading-Edge Camber on Low-Speed Characteristics of Slender Delta Wings," NASA CR-2002, 1979.

[28] Kirkpatrick, D.L.I., "Analysis of the Static Pressure Distribution on a Delta Wing in Subsonic Flow," Aeronautical Research Council, R&M 3619, Aug. 1968.

[29] Fox, C. H. Jr. and Lamar, J. E., "Theoretical and Experimental Longitudinal Aerodynamic Characteristics of an Aspect Ratio 0.25 Sharp-Edge Delta Wing at Subsonic, Supersonic, and Hypersonic Speeds," NASA TN D-7651, Aug. 1974.

[30] Bartlett, G. E. and Vidal, R. J., "Experimental Investigation of Influence of Edge Shape on the Aerodynamic Characteristics of Low Aspect Ratio Wings at Low Speeds," *Journal of Aerospace Sciences*, Vol. 22, Aug. 1955, pp. 517-533.

[31] Hummel, D., "On the Vortex Formation over a Slender Wing at Large Angles of Incidence," Paper 15, AGARD-CP-247, Jan. 1979.

[32] Lamar, J. E., "Extension of Leading-Edge Suction Analogy to Wings with Separated Flow around the Side Edges at Subsonic Speeds," NASA TR R-428, Oct. 1974.